Molecular dynamics simulation study of N-methylacetamide in water. II. Two-dimensional infrared pump–probe spectra

Cite as: J. Chem. Phys. **119**, 2256 (2003); https://doi.org/10.1063/1.1580808
Submitted: 24 February 2003 . Accepted: 16 April 2003 . Published Online: 11 July 2003

Kijeong Kwac, and Minhaeng Cho

Molecular dynamics simulation study of *N*-methylacetamide in water. II. Two-dimensional infrared pump–probe spectra

Kijeong Kwac and Minhaeng Cho[a)]
Department of Chemistry and Center for Multidimensional Spectroscopy, Division of Chemistry and Molecular Engineering, Korea University, Seoul 136-701, Korea

(Received 24 February 2003; accepted 16 April 2003)

A theoretical description of two-dimensional (2D) IR pump–probe spectroscopy of a three-level system is presented by taking into account the system–bath interaction. By using the correlation function of the fluctuating amide I mode frequency of *N*-methylacetamide in D_2O, which was obtained by carrying out both *ab initio* calculations and MD simulations, the time-resolved 2D pump–probe spectra as a function of pump–probe pulse delay time are calculated and compared with experiment. We found that the vibrational dephasing becomes homogeneous on the 2 ps time scale, which is a bit faster than the experimental result. It is theoretically shown that the degree of slant of 2D contours is linearly proportional to the correlation function of the fluctuating amide I mode frequency. Consequently, it is suggested that the 2D IR pump–probe spectroscopy can provide a direct information on the vibrational frequency fluctuation dynamics and on the magnitude of static inhomogeneity. © *2003 American Institute of Physics.* [DOI: 10.1063/1.1580808]

I. INTRODUCTION

Amide I vibration of a peptide is strongly IR active and has known to be coupled to other local amide I modes to form delocalized normal modes.[1–15] Furthermore, its frequency is very sensitive to the solvent polarity, as shown by Eaton *et al.*[16] using IR absorption spectroscopy for *N*-methylacetamide (NMA) dissolved in a variety of protic and aprotic solvents. In addition to the one-dimensional vibrational spectroscopies such as IR absorption and Raman scattering spectroscopies, 2D IR pump–probe (PP) and photon echo methods have been used to study vibrational dynamics and spectral evolution of the amide I bands of various polypeptides.[17–24] Since these 2D vibrational spectroscopic techniques can provide quantitatively reliable information on the solvation effects on the amide I mode frequency fluctuation and interpeptide couplings, it became possible to use them to determine three-dimensional structures of small polypeptides in solutions.[17–25]

Recently, Woutersen *et al.*[24] carried out 2D IR PP experiments of both trialanine and NMA in water and showed that there exists two different trialanine conformations and that the amide I mode frequency becomes homogeneous on the 4 ps time scale. There is no truly static inhomogeneity in solution, but the dynamical inhomogeneity exists for a very short time. The dynamical inhomogeneity means that the solvent configurations around different solutes can be considered to be inhomogeneously distributed if the time scale is sufficiently short in comparison to the solvent correlation time of the relevant fluctuating variable, which is in this case the fluctuating amide I mode frequency. Stock, Hamm, and co-workers[26] carried out classical MD simulation studies of NMA in liquid methanol and suggested that two distinctively different hydrogen-bonding structures of NMA exist and are likely to be separated by a certain potential barrier. This observation was used to explain why the amide I IR band of NMA in methanol solution is doublet. However, as discussed in Ref. 27, which will be referred to as Paper I throughout this paper, the classical MD simulation with conventional intermolecular potential functions may not be quantitatively reliable for describing amide I mode frequency shift and fluctuation amplitude. More specifically, we showed that the Coulomb and Lennard-Jones interaction potentials cannot be used to reproduce the experimentally measured amide I mode frequency redshift of 81 cm^{-1}.[16,27]

Recently, we presented a theoretical description of the amide I mode frequencies of 96 different NMA–$n D_2O$ complexes, where the amide I mode frequencies were calculated by using *ab initio* calculation methods and by applying the multivariate least square regression method.[28] Using the same empirical formula reported in Ref. 28 to quantitatively calculate the instantaneous amide I mode frequency of NMA in liquid water, we were able to quantitatively determine the solvatochromic amide I mode frequency shift and its fluctuation amplitude.[27] Then, the theoretically predicted IR absorption line shape was found to be in good agreement with experiment.

In the present paper, we will use the same MD simulation results to numerically calculate 2D IR pump–probe spectra of NMA dissolved in D_2O, and compare them with Woutersen *et al.*'s experimental results.[24] In Sec. II, a theoretical description of the 2D IR PP spectroscopy will be presented. Numerical calculation results will be discussed in detail in Sec. III. Finally, the main results will be summarized in Sec. IV.

II. TWO-DIMENSIONAL IR PUMP–PROBE RESPONSE FUNCTION

In Ref. 29, one of the authors presented a detailed theoretical description of the 2D IR PP spectroscopy and corresponding response functions in the vibrational eigenstate rep-

a)Electronic mail: mcho@korea.ac.kr

resentation. In the present paper, we will briefly outline the main results for the sake of completeness.

For a multilevel system, the most general 3D vibrational response function, when the electric-dipole-field interactions are only taken into account, is written as

$$R_{3D}(t_3,t_2,t_1)\equiv\left(\frac{i}{\hbar}\right)^3\theta(t_1)\theta(t_2)\theta(t_3)\langle[[[\mu(t_3+t_2+t_1),\mu(t_2+t_1)],\mu(t_1)],\mu(0)]\rho_0\rangle. \quad (1)$$

Here, the Heaviside step function was denoted as $\theta(t)$ and ρ_0 is the initial equilibrium density operator. The time-dependence of each operator is determined by the Heisenberg equation of motion so that $\hat{x}(t)\equiv e^{iHt/\hbar}\hat{x}e^{-iHt/\hbar}$. Expanding the three commutators in Eq. (1), we have

$$R_{3D}(t_3,t_2,t_1)=\left(\frac{i}{\hbar}\right)^3\theta(t_1)\theta(t_2)\theta(t_3)\sum_{\alpha=1}^{4}[R_\alpha(t_3,t_2,t_1)-R_\alpha^*(t_3,t_2,t_1)], \quad (2)$$

where the four components are

$$\begin{aligned}
R_1(t_3,t_2,t_1)&\equiv\langle\mu(t_1)\mu(t_1+t_2)\mu(t_1+t_2+t_3)\mu(0)\rho_0\rangle,\\
R_2(t_3,t_2,t_1)&\equiv\langle\mu(0)\mu(t_1+t_2)\mu(t_1+t_2+t_3)\mu(t_1)\rho_0\rangle,\\
R_3(t_3,t_2,t_1)&\equiv\langle\mu(0)\mu(t_1)\mu(t_1+t_2+t_3)\mu(t_1+t_2)\rho_0\rangle,\\
R_4(t_3,t_2,t_1)&\equiv\langle\mu(t_1+t_2+t_3)\mu(t_1+t_2)\mu(t_1)\mu(0)\rho_0\rangle.
\end{aligned} \quad (3)$$

For a given nonlinear response function, the corresponding polarization can be in general written as

$$\mathbf{P}(\mathbf{r},t)=N\int_0^\infty dt_3\int_0^\infty dt_2\int_0^\infty dt_1 R_{3D}(t_3,t_2,t_1)\mathbf{E}(\mathbf{r},t-t_3)\times\mathbf{E}(\mathbf{r},t-t_3-t_2)\times\mathbf{E}(\mathbf{r},t-t_3-t_2-t_1), \quad (4)$$

where N is the chromophore number density. In Eq. (4), $\mathbf{E}$ is the external electric field treated as a classical function.

For the IR PP spectroscopy, if the two pulses are well separated in time, the first two field–matter interactions are with the pump pulse and followed by the third interaction with the probe field to create the third-order polarization. Then, the weak probe difference absorption signal, which is defined as the difference between the pump–probe signal and the probe-only signal, is given as, within the lowest-order perturbation theory,

$$S_{PP}(\omega_{pr},\omega_{pu};T)=A(\omega_{pr})\mathrm{Im}\int_{-\infty}^{\infty}dt\mathbf{E}_{pr}^*(\mathbf{k}_{pr},t)\cdot\mathbf{P}_{PP}(\mathbf{k}_s,t;T), \quad (5)$$

where the auxiliary function, $A(\omega_{pr})$, is defined as

$$A(\omega_{pr})\equiv\frac{4\pi\omega_{pr}}{cn(\omega_{pr})}\left[\int_{-\infty}^{\infty}dt|\mathbf{E}_{pr}(\mathbf{k}_{pr},t)|^2\right]^{-1}. \quad (6)$$

The refractive index was denoted as n. The pump and probe center frequencies are ω_{pu} and ω_{pr}, respectively. The delay time between the pump and probe pulses is denoted as T. The third-order PP polarization $\mathbf{P}_{PP}(\mathbf{k}_s,t;T)$ is the corresponding wave-vector ($\mathbf{k}_s=\mathbf{k}_2$) component of the third-order polarization. The pump and probe fields are given as

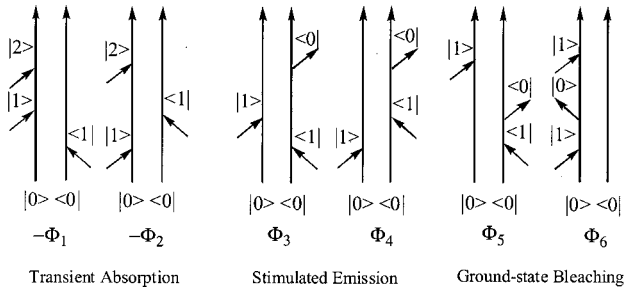

FIG. 1. Double-sided Feynman diagrams associated with the PP spectroscopy of a three-level system. Only the case when the pump and probe pulses are well-separated in time was considered.

$$\begin{aligned}
\mathbf{E}_{pu}(\mathbf{r},t)&=\mathbf{u}_{pu}f_{pu}(t)e^{i\mathbf{k}_{pu}\cdot\mathbf{r}-i\omega_{pu}t}+\text{c.c.},\\
\mathbf{E}_{pr}(\mathbf{r},t)&=\mathbf{u}_{pr}f_{pr}(t)e^{i\mathbf{k}_{pr}\cdot\mathbf{r}-i\omega_{pr}t}+\text{c.c.},
\end{aligned} \quad (7)$$

where $\mathbf{u}_{pu}$ and $\mathbf{u}_{pu}$ are the unit vectors of the two field polarization directions. The pulse envelope function, which is assumed to be real, was denoted as $f(t)$.

A. Nonlinear response function of a three-state system

The amide I vibrational quantum states of NMA in D_2O can be approximated to be a three-state system, i.e., $|0\rangle$, $|1\rangle$, and $|2\rangle$. The overtone (second vibrationally excited) state is $|2\rangle$. For this three-level system, within the rotating-wave-approximation, there are six double-sided Feynman diagrams directly associated with the IR PP spectroscopy (in Fig. 1). The first two contributions, Φ_1 and Φ_2, are the so-called transient absorption terms. The third and fourth contributions, Φ_3 and Φ_4, are the stimulated emission terms. The fifth and sixth contributions, Φ_5 and Φ_6, are the ground-state bleaching terms. Each of these six contributions correspond to one of the four nonlinear response functions (R_1-R_4) given in Eq. (7) of Ref. 29 as

$$\begin{aligned}
\Phi_1(t_3,t_2,t_1)&=-R_1^*(t_3,t_2,t_1)\\
&\quad(\text{with } |a\rangle=|0\rangle,|b\rangle=|d\rangle=|1\rangle, \text{ and } |c\rangle=|2\rangle),\\
\Phi_2(t_3,t_2,t_1)&=-R_2^*(t_3,t_2,t_1)\\
&\quad(\text{with } |a\rangle=|0\rangle,|b\rangle=|d\rangle=|1\rangle, \text{ and } |c\rangle=|2\rangle),\\
\Phi_3(t_3,t_2,t_1)&=R_2(t_3,t_2,t_1)\\
&\quad(\text{with } |a\rangle=|c\rangle=|0\rangle \text{ and } |b\rangle=|d\rangle=|1\rangle),\\
\Phi_4(t_3,t_2,t_1)&=R_1(t_3,t_2,t_1)\\
&\quad(\text{with } |a\rangle=|c\rangle=|0\rangle \text{ and } |b\rangle=|d\rangle=|1\rangle),\\
\Phi_5(t_3,t_2,t_1)&=R_3(t_3,t_2,t_1)\\
&\quad(\text{with } |a\rangle=|c\rangle=|0\rangle \text{ and } |b\rangle=|d\rangle=|1\rangle),\\
\Phi_6(t_3,t_2,t_1)&=R_4(t_3,t_2,t_1)\\
&\quad(\text{with } |a\rangle=|c\rangle=|0\rangle \text{ and } |b\rangle=|d\rangle=|1\rangle).
\end{aligned} \quad (8)$$

In order to calculate the six response functions in Eqs. (8), we need to determine the following four correlation functions:

$$\begin{aligned}
\xi_{11}(\tau_1,\tau_2) &\equiv \langle \delta\Omega_{10}(\tau_1)\,\delta\Omega_{10}(\tau_2)\rangle,\\
\xi_{22}(\tau_1,\tau_2) &\equiv \langle \delta\Omega_{20}(\tau_1)\,\delta\Omega_{20}(\tau_2)\rangle,\\
\xi_{12}(\tau_1,\tau_2) &\equiv \langle \delta\Omega_{10}(\tau_1)\,\delta\Omega_{20}(\tau_2)\rangle,\\
\xi_{21}(\tau_1,\tau_2) &\equiv \langle \delta\Omega_{20}(\tau_1)\,\delta\Omega_{10}(\tau_2)\rangle,
\end{aligned} \tag{9}$$

where $\delta\Omega_{j0}(t)$ denotes the fluctuating part of the transition frequency operator between $|j\rangle$ and $|0\rangle$. As discussed in Paper I, the solute–solvent interaction induces fluctuation of the force constant of the NMA amide I mode. For a weakly anharmonic oscillator, one can assume that $\delta\Omega_{20}(t) \cong 2\,\delta\Omega_{10}(t)$. Then, we have

$$\begin{aligned}
\xi(\tau_1,\tau_2) \equiv \xi_{11}(\tau_1,\tau_2) &= \tfrac{1}{4}\xi_{22}(\tau_1,\tau_2)\\
&= \tfrac{1}{2}\xi_{12}(\tau_1,\tau_2) = \tfrac{1}{2}\xi_{21}(\tau_1,\tau_2)
\end{aligned}$$

and

$$\xi(\tau_1-\tau_2) = \xi(\tau_1,\tau_2) = \langle \delta\Omega(\tau_1-\tau_2)\,\delta\Omega(0)\rangle, \tag{10}$$

where the transition frequency operator between $|1\rangle$ and $|0\rangle$ was denoted as $\delta\Omega$. Here, the fuctuating frequencies in the above equations are quantum mechanical operators and $\langle\cdots\rangle$ means the trace over the correspoding eigenstates. Therefore, $\xi(t)$ is a complex function and cannot be directly obtained from the classical MD trajectories. However, by using the fluctuation–dissipation relationship[30] and invoking semiclassical approximation, it becomes possible to obtain an approximate $\xi(t)$.[27] Then, the six relevant response functions can be written in terms of the linear line-broadening function $g(t)$ as

$$\begin{aligned}
\Phi_1(t_3,t_2,t_1) &= -P(0)\mu_{01}\mu_{12}\mu_{21}\mu_{10}\exp\{-i\bar{\omega}_{21}t_3 + i\bar{\omega}_{10}t_1\}\\
&\quad\times\Gamma_{\mathrm{TA}}(t_3,t_2,t_1)\exp\{-g(t_3)-g^*(t_1)+g(t_2)\\
&\quad - g^*(t_1+t_2)-g(t_2+t_3)+g^*(t_1+t_2+t_3)\},\\
\Phi_2(t_3,t_2,t_1) &= -P(0)\mu_{01}\mu_{12}\mu_{21}\mu_{10}\\
&\quad\times\exp\{-i\bar{\omega}_{21}t_3 - i\bar{\omega}_{10}t_1\}\Gamma_{\mathrm{TA}}(t_3,t_2,t_1)\\
&\quad\times\exp\{-g(t_3)-g(t_1)-g^*(t_2)+g(t_1+t_2)\\
&\quad + g^*(t_2+t_3)-g(t_1+t_2+t_3)\},\\
\Phi_3(t_3,t_2,t_1) &= P(0)\mu_{01}\mu_{10}\mu_{01}\mu_{10}\\
&\quad\times\exp\{-i\bar{\omega}_{10}t_3 + i\bar{\omega}_{10}t_1\}\Gamma_{\mathrm{SE}}(t_3,t_2,t_1)\\
&\quad\times\exp\{-g^*(t_3)-g^*(t_1)+g(t_2)\\
&\quad - g^*(t_1+t_2)-g(t_2+t_3)+g^*(t_1+t_2+t_3)\},\\
\Phi_4(t_3,t_2,t_1) &= P(0)\mu_{01}\mu_{10}\mu_{01}\mu_{10}\\
&\quad\times\exp\{-i\bar{\omega}_{10}t_3 - i\bar{\omega}_{10}t_1\}\Gamma_{\mathrm{SE}}(t_3,t_2,t_1)\\
&\quad\times\exp\{-g^*(t_3)-g(t_1)-g^*(t_2)\\
&\quad + g(t_1+t_2)+g^*(t_2+t_3)-g(t_1+t_2+t_3)\},
\end{aligned} \tag{11}$$

$$\begin{aligned}
\Phi_5(t_3,t_2,t_1) &= P(0)\mu_{01}\mu_{10}\mu_{01}\mu_{10}\\
&\quad\times\exp\{-i\bar{\omega}_{10}t_3 + i\bar{\omega}_{10}t_1\}\Gamma_{\mathrm{GB}}(t_3,t_2,t_1)\\
&\quad\times\exp\{-g(t_3)-g^*(t_1)+g^*(t_2)\\
&\quad - g^*(t_1+t_2)-g^*(t_2+t_3)+g^*(t_1+t_2+t_3)\},\\
\Phi_6(t_3,t_2,t_1) &= P(0)\mu_{01}\mu_{10}\mu_{01}\mu_{10}\\
&\quad\times\exp\{-i\bar{\omega}_{10}t_3 - i\bar{\omega}_{10}t_1\}\Gamma_{\mathrm{GB}}(t_3,t_2,t_1)\\
&\quad\times\exp\{-g(t_3)-g(t_1)-g(t_2)+g(t_1+t_2)\\
&\quad + g(t_2+t_3)-g(t_1+t_2+t_3)\},
\end{aligned}$$

where a detailed procedure to calculate $g(t)$ by means of MD simulation was presented in Paper I. Here, the population of the excited states are assumed to be negligibly smaller than that of the ground state, i.e., $P(n\geqslant 1) \ll P(0)$. The vibrational transition dipole matrix element, e.g., μ_{ba}, is defined as $\mu_{ba} \equiv \langle b|\mu|a\rangle$. Denoting the inverse lifetimes of the first and second excited states as γ_1 and γ_2, respectively, we find that the lifetime-broadening factors are given as

$$\begin{aligned}
\Gamma_{\mathrm{TA}}(t_3,t_2,t_1) &= \exp\left\{-\frac{(\gamma_1+\gamma_2)t_3}{2} - \gamma_1 t_2 - \frac{\gamma_1 t_1}{2}\right\},\\
\Gamma_{\mathrm{SE}}(t_3,t_2,t_1) &= \exp\left\{-\frac{\gamma_1 t_3}{2} - \gamma_1 t_2 - \frac{\gamma_1 t_1}{2}\right\},\\
\Gamma_{\mathrm{GB}}(t_3,t_2,t_1) &= \exp\left\{-\frac{\gamma_1 t_3}{2} - \gamma_1 t_2 - \frac{\gamma_1 t_1}{2}\right\}.
\end{aligned} \tag{12}$$

B. IR pump–probe spectrum

Although the IR pump and probe pulses used in an experiment have finite widths, we will consider an ideal snapshot limit to study the time evolution of the IR pump–probe spectrum of NMA in solutions. Then, the two-dimensional IR pump–probe spectrum is given by a sum of the three distinctive spectra, i.e.,

$$\begin{aligned}
S_{\mathrm{PP}}(\omega_{\mathrm{pr}},\omega_{\mathrm{pu}};T) \propto -\mathrm{Re}[&\Psi_{\mathrm{TA}}(\omega_{\mathrm{pr}},\omega_{\mathrm{pu}};T)\\
&+\Psi_{\mathrm{SE}}(\omega_{\mathrm{pr}},\omega_{\mathrm{pu}};T)\\
&+\Psi_{\mathrm{GB}}(\omega_{\mathrm{pr}},\omega_{\mathrm{pu}};T)],
\end{aligned} \tag{13}$$

where the three terms on the right-hand side of Eq. (13) correspond to the transient absorption, stimulated emission, and ground-state bleaching contributions, respectively, and they are

$$\begin{aligned}
\Psi_{\mathrm{TA}}(\omega_{\mathrm{pr}},\omega_{\mathrm{pu}};T) &= \tilde{\Phi}_1(\omega_{\mathrm{pr}},\omega_{\mathrm{pu}};T) + \tilde{\Phi}_2(\omega_{\mathrm{pr}},\omega_{\mathrm{pu}};T),\\
\Psi_{\mathrm{SE}}(\omega_{\mathrm{pr}},\omega_{\mathrm{pu}};T) &= \tilde{\Phi}_3(\omega_{\mathrm{pr}},\omega_{\mathrm{pu}};T) + \tilde{\Phi}_4(\omega_{\mathrm{pr}},\omega_{\mathrm{pu}};T),\\
\Psi_{\mathrm{GB}}(\omega_{\mathrm{pr}},\omega_{\mathrm{pu}};T) &= \tilde{\Phi}_5(\omega_{\mathrm{pr}},\omega_{\mathrm{pu}};T) + \tilde{\Phi}_6(\omega_{\mathrm{pr}},\omega_{\mathrm{pu}};T).
\end{aligned} \tag{14}$$

The six 2D spectra associated with the six pathways in Fig. 1 are defined as

$$\begin{aligned}
\tilde{\Phi}_1(\omega_{\mathrm{pr}},\omega_{\mathrm{pu}};T) = \int_0^\infty dt_3 \int_0^\infty dt_1 \exp(&i\omega_{\mathrm{pr}}t_3\\
&- i\omega_{\mathrm{pu}}t_1)\Phi_1(t_3,t_2=T,t_1),
\end{aligned}$$

$$\tilde{\Phi}_2(\omega_{\rm pr},\omega_{\rm pu};T)=\int_0^\infty dt_3\int_0^\infty dt_1\exp(i\omega_{\rm pr}t_3+i\omega_{\rm pu}t_1)\Phi_2(t_3,t_2=T,t_1),$$

$$\tilde{\Phi}_3(\omega_{\rm pr},\omega_{\rm pu};T)=\int_0^\infty dt_3\int_0^\infty dt_1\exp(i\omega_{\rm pr}t_3-i\omega_{\rm pu}t_1)\Phi_3(t_3,t_2=T,t_1),$$

$$\tilde{\Phi}_4(\omega_{\rm pr},\omega_{\rm pu};T)=\int_0^\infty dt_3\int_0^\infty dt_1\exp(i\omega_{\rm pr}t_3+i\omega_{\rm pu}t_1)\Phi_4(t_3,t_2=T,t_1),$$

$$\tilde{\Phi}_5(\omega_{\rm pr},\omega_{\rm pu};T)=\int_0^\infty dt_3\int_0^\infty dt_1\exp(i\omega_{\rm pr}t_3-i\omega_{\rm pu}t_1)\Phi_5(t_3,t_2=T,t_1),$$

$$\tilde{\Phi}_6(\omega_{\rm pr},\omega_{\rm pu};T)=\int_0^\infty dt_3\int_0^\infty dt_1\exp(i\omega_{\rm pr}t_3+i\omega_{\rm pu}t_1)\Phi_6(t_3,t_2=T,t_1). \quad (15)$$

In the following section, we will present numerically calculated 2D PP spectra of NMA in water using Eqs. (13)–(15).

III. NUMERICAL CALCULATION RESULTS OF 2D IR PUMP–PROBE SPECTRA

In this section, we will present numerically calculated 2D IR PP spectra and compare them with those predicted by using two parameter sets determined by Woutersen *et al.*[24] and by Zanni *et al.*[21] independently.

In order to numerically calculate the six components in Eqs. (11), we will assume that $\mu_{21}=\mu_{12}=\sqrt{2}\mu_{10}=\sqrt{2}\mu_{01}$ throughout this paper. Also, the anharmonicity is assumed to be 16 $\rm cm^{-1}$ so that $(\bar{\omega}_{10}-\bar{\omega}_{21})/2\pi c=16\ \rm cm^{-1}$, where c is the speed of light in cm/s.

A. Parameters used in Ref. 24

Woutersen *et al.*[24] carried out 2D IR PP experiments of an NMAD in D_2O. They assumed that the amide I mode frequency fluctuation correlation function, denoted as $\xi(t)$ in the present paper, was real and assumed to be given as a sum of two components, i.e.,

$$\xi_W(t)=\frac{\delta(t)}{T_2^*}+\Delta_1^2\exp(-t/\tau_c), \quad (16)$$

where the pure-dephasing constant T_2^* is 800 fs. The delta function part was used to model the ultrafast inertial component and the slowly decaying exponential function, the second term on the right-hand side of Eq. (16), was introduced to model the diffusive component. Here, the root mean square of the amide I mode frequency fluctuation, Δ_1, and correlation time, τ_c, were obtained by fitting and are 9 $\rm cm^{-1}$ and 1600 fs, respectively. Equation (16) contains a relatively slowly decaying component in comparison to our $\xi(t)$. Now, in order to calculate 2D PP spectra, the lifetimes of $|1\rangle$ and $|2\rangle$ states are to be determined. In Ref. 24, they assumed that $\gamma_1=1\ \rm ps^{-1}$ and $\gamma_2=2\ \rm ps^{-1}$.

B. Parameters used in Ref. 21

Zanni *et al.*[21] reported heterodyne-detected stimulated IR photon echo spectra of an NMAD in D_2O to study dynamical fluctuation effect on the 2D spectrum. In order to interpret their experimentally measured 2D spectrum, they used the following form of $\xi(t)$:

$$\xi_Z(t)=\Delta_1^2\exp(-t/\tau_1)+\Delta_0^2, \quad (17)$$

where $\Delta_1=12.2\ \rm ps^{-1}$, $\tau_1=6$ fs, and $\Delta_0=1.1\ \rm ps^{-1}$. On the basis of the pump–probe experiment, the lifetimes of the first and second excited states were estimated to be 450 and 310 fs so that $\gamma_1=2.22\ \rm ps^{-1}$ and $\gamma_2=3.23\ \rm ps^{-1}$. Note that these two values differ from those used in Ref. 24.

In comparison to Woutersen *et al.*'s $\xi(t)$, Zanni *et al.*'s exponentially decaying component is extremely fast, though they introduced this 6 fs exponential function to model the ultrafast inertial component.[21] Furthermore, Zanni *et al.*[21] introduced a static inhomogeneity of which width is determined by Δ_0. Nevertheless, they were able to successfully reproduce their IR photon echo spectra by using the above functional form of $\xi(t)$.

C. Numerically calculated IR pump–probe spectra

In this subsection, we will present numerically calculated 2D IR PP spectra by using theoretical expressions in Sec. II and $\xi(t)$ obtained in Paper I. In order to take into account the lifetime broadening contribution, we will use the same inverse lifetimes estimated by Hochstrasser and coworkers in Ref. 21, i.e., $\gamma_1=2.22\ \rm ps^{-1}$ and $\gamma_2=3.23\ \rm ps^{-1}$. However, when we calculate the 2D spectra by using Woutersen *et al.*'s $\xi_W(t)$, we will use the lifetimes reported in their paper, i.e., $\gamma_1=1\ \rm ps^{-1}$ and $\gamma_2=2\ \rm ps^{-1}$. Also, as shown by Woutersen *et al.*,[24] the spectral diffusion contribution was not observed in their experiment so that we will ignore the imaginary part of $\xi(t)$ in the following calculations.

In Fig. 2, the numerically calculated 2D IR pump–probe spectra are plotted. The five spectra in the first column (A) of Fig. 2 are those predicted by using the MD simulation results and they correspond to the cases when the delay times are 200, 400, 800, 2000, and 4000 fs, respectively. Those in the second column (B) were calculated by using the Woutersen *et al.*'s parameters,[24] whereas those in the third column (C) were by using the Zanni *et al.*'s parameters.[21] Note that these three sets of spectra appear to be distinctively different from one another. The experimentally measured 2D IR spectra are quantitatively similar to those in the second column of Fig. 2, since $\xi(t)$ and required parameters were determined by fitting their 2D IR pump–probe spectra in Ref. 24.

The positive peak located at $\omega_{\rm pu}=1627\ \rm cm^{-1}$ and $\omega_{\rm pr}=1602\ \rm cm^{-1}$ is from the transient absorption from $|1\rangle$ to $|2\rangle$, and the negative peak at $\omega_{\rm pu}=\omega_{\rm pr}=1627\ \rm cm^{-1}$ is from both the stimulated emission and ground-state bleaching contributions. Since the transition frequency is inhomogeneouly distributed for such a short time (200 fs), the contours are not vertically directed. As shown by Woutersen *et al.*,[24] this deviation from the vertically directed contours is a clear evidence of the memory survived over the population evolution period T. That is to say, if the pure dephasing is approxi-

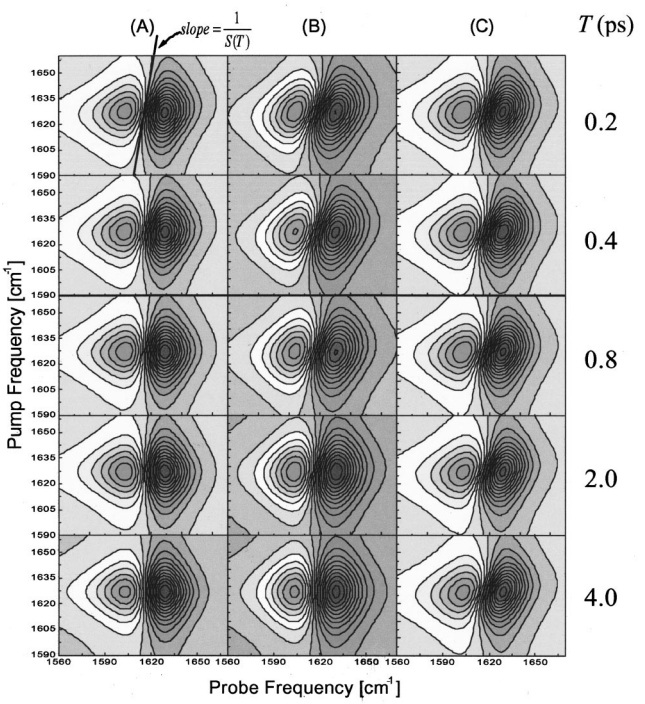

FIG. 2. Numerically calculated 2D IR PP spectra. The delay time T varies from 200, 400, 800, 2000, to 4000 fs from top to bottom. The spectra in the first column were calculated by using the MD simulated $\xi(t)$. Those in the second and third columns were obtained by using Eqs. (24) and (25), respectively. The inverse lifetimes of the first and second excited states used in the present calculations are given in the context.

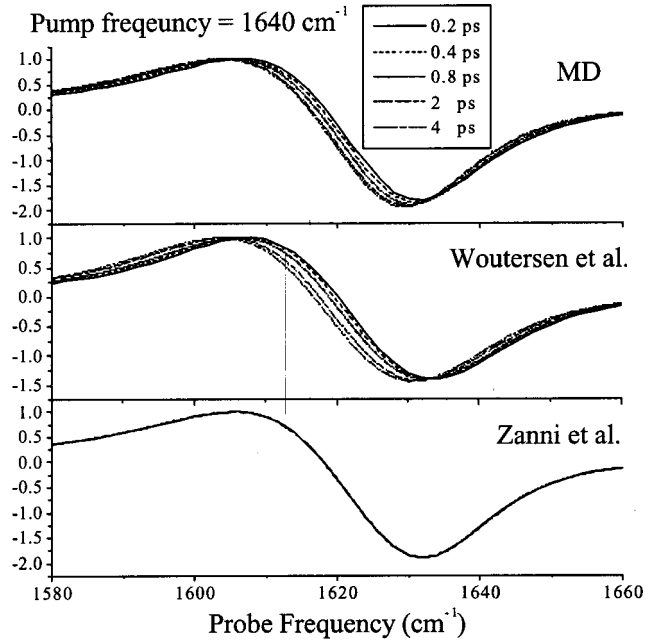

FIG. 3. The slices of the 2D IR PP spectra in Fig. 2 are plotted, when the pump field frequency equals 1640 cm^{-1}. As the pump–probe pulse delay time increases, the spectrum with respect to the probe field frequency exhibits a redshifting behavior.

mated to be Markovian, the contours are vertically directed regardless of the delay time. As can be seen in our 2D spectrum at $T=2000$ fs, the amide I band of NMA in D_2O becomes homogeneous on this time scale. However, Woutersen *et al.*[24] observed that the time scale for the homogeneous dephasing is about 4 ps. Note that the contours [see the fifth panel in the column (B) of Fig. 2] are vertically directed when the delay time is 4 ps. In order to take into account this long-lasting memory effect, Woutersen *et al.* had to use an exponentially decaying function for $\xi(t)$ with a decay constant of 1.6 ps. However, our $M(t)$ from MD simulation does not contain this slowly decaying component so that the time scale for the homogeneous dephasing is slightly less than the experimental result.

Now, let us examine the 2D spectra calculated by using Zanni *et al.*'s $\xi(t)$ (Ref. 21) [see those in column (C) of Fig. 2]. Although the intensity of the signal decreases as the delay time increases, the 2D contours appear to be insensitive to the delay time at all. Furthermore, the contours are not vertically directed at all times. These results can be understood by noting (i) that the exponentially decaying component in $\xi(t)$ of which decay constant was assumed to be 6 fs is much smaller than the delay time and (ii) that there is a static inhomogeneous contribution to the amide I mode frequency fluctuation. Due to the latter aspect, the contours would never become vertically directed. This means that the 2D IR pump–probe spectrum is highly sensitive to the long-time behavior of the vibrational frequency fluctuation in solution. Nevertheless, the observation that there appears significant disagreement between columns (B) and (C) in Fig. 2 does not mean that the vibrational photon echo method may not be so useful in the determination of the frequency autocorrelation function, in comparison to the IR pump–probe method. As emphasized in the present paper as well as clearly noted by Woutersen *et al.* in Ref. 24, the 2D IR pump–probe spectrum is found to be sensitive to the existence of the (short-time, conformational, or truly static) inhomogeneity because the tilting behavior of the 2D spectrum is visible and easily recognizable.

In Fig. 3, the five slices of the 2D IR PP spectra in Fig. 2 are plotted as a function of pump–probe delay time. The spectrum is normalized by making the maximum value to be a unity. The overall shapes of the 1D spectra obtained by using the present MD simulation method are quantitatively in good agreement with those of Woutersen *et al.*'s model. Consequently, in addition to the good agreement between simulated and measured 1D absorption spectra, the present MD simulation method developed in Papers I and II were found to be reliable in reproducing the experimentally measured 2D IR PP spectra.

In order to quantify the degree of slant of the contours, we considered the inverse slope of the tangential line of the 2D contours in the middle of positive and negative peaks of the 2D spectrum, denoted as $S(T)$, as a function of the delay time T. The slant linear line in Fig. 2 is written as

$$\omega_{\mathrm{pu}}=\frac{1}{S(T)}\omega_{\mathrm{pr}}+C, \tag{18}$$

where $S(T)$ is the inverse slope of that line and C is a constant. In the Appendix, we theoretically proved that $S(T)$ is

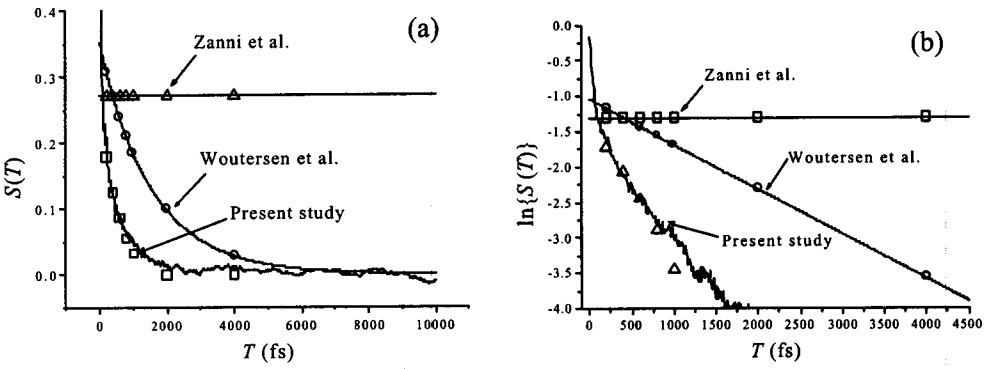

FIG. 4. $S(T)$ vs T. The $S(T)$ value was numerically calculated from the associated 2D IR PP spectra in Fig. 2. The plot of $\ln S(T)$ vs T is shown in (b). The scaled $\xi(t)$'s are also plotted in these figures to show that indeed $S(T)$ is linearly proportional to $\xi(t)$.

always less than a unity and is linearly proportional to $\xi(T)$, i.e.,

$$S(T) \propto \xi(T). \tag{19}$$

In Fig. 4(a), numerically estimated $S(T)$ from Fig. 2 is plotted for the three cases. As expected, if Zanni *et al.*'s parameters[21] are used, $S(T)$ does not dependent on the delay time in the range from 200 to 4000 fs. On the other hand, our $S(T)$ decays too fast in comparison to that obtained by using Woutersen *et al.*'s parameters.[24] In Fig. 4(b), we also plot $\ln\{S(T)\}$ versus T. The exponential decay for the case of Woutersen *et al.*'s model[24] is evident, whereas our $S(T)$ is slightly deviated from an exponential function because the MD simulated $\xi(T)$ does not decay like an exponential function.

The linear relationship between experimentally measurable $S(T)$ and $\xi(T)$ suggests that one can directly measure the correlation function of the fluctuating vibrational frequency in general by using the 2D IR PP spectroscopy. Thus, chromophore-solvent-interaction-induced fluctuation dynamics of not only the amide I mode considered in the present paper but also any intramolecular vibrational degree of freedom that is coupled to bath modes can be studied by carefully analyzing the time evoluation of 2D IR PP spectra as a function of pump–probe pulse delay time.

Before we close this section, it should be mentioned that recently Piryatinski and Skinner theoretically showed that the slope of the initial photon echo signal at $t_1=0$ is linearly proportional to the same frequency autocorrelation function, $\xi(T)$.[31] This is an extention of the photon echo peak shift measurement method.[32] Thus, if one would carry out a stimulated photon echo experiment and measure either the initial slope of the echo signal or the photon echo peak shift, the fluctuating frequency correlation function can be experimentally measured and compared with that obtained from the time-resolved 2D IR PP contours.

IV. SUMMARY AND A FEW CONCLUDING REMARKS

By using the theory in Ref. 29, the 2D IR PP signal of a three-level system that is coupled to bath degrees of freedom was theoretically derived and presented in Eqs. (13)–(15). Using the correlation function of the fluctuating amide I mode frequency of NMA in D_2O, which was obtained by carrying out MD simulations and *ab initio* calculations, we calculated time-resolved 2D IR PP spectra and compared them with the experimental results reported by Woutersen *et al.*[24] Also, these two series of spectra are compared with those calculated by using Zanni *et al.*'s parameters[21] determined by fitting their IR photon echo spectra. Our 2D IR PP spectra show that the vibrational dephasing becomes homogeneous on the 2 ps time scale, which is a bit faster than the experimental result. Nevertheless, due to the long-lasting memory survived over the population evolution period, the 2D contours were not vertically directed in the range from 200 to 2000 fs. By using a short-time approximation to the line shape function, $g(t)$, we proved that the degree of slant of 2D contours is not only found to be a function of the pump–probe pulse delay time, T, but also linearly proportional to the correlation function of the fluctuating amide I mode frequency. On the basis of this theoretical result, it was suggested that the 2D IR pump–probe spectroscopy can provide direct and quantitative information on the vibrational frequency fluctuation dynamics as well as the existence of inhomogeneous contribution to the vibrational line broadening.

ACKNOWLEDGMENT

This work was supported by the Creative Research Initiatives Program of KISTEP (MOST, Korea).

APPENDIX: CALCULATION OF THE 2D CONTOUR SLANT, $S(T)$

As can be seen in Fig. 2, the contours are slant when the pulse delay time is comparable to the time scale of $\xi(T)$. In this Appendix, we will theoretically show that the inverse slope of the linear line drawn in Fig. 2 (see the top-left pannel), denoted as $S(T)$, is linearly proportional to $\xi(T)$.

In order to achieve this goal, we will assume that the line shape function, $g(t)$, is real, that is to say, the spectral diffusion contribution is negligibly small. Indeed, this is the case of the system (NMA in D_2O) considered in the present paper. Now, one can take the following short-time approximations with respect to t_1 and t_3:

$$g(t_1)\cong \tfrac{1}{2}\Delta^2 t_1^2,$$

$$g(t_3)\cong \tfrac{1}{2}\Delta^2 t_3^2,$$

$$g(t_1+t_2)\cong g(t_2)+\tfrac{1}{2}\xi(t_2)t_1^2, \tag{A1}$$

$$g(t_2+t_3)\cong g(t_2)+\tfrac{1}{2}\xi(t_2)t_3^2,$$

$$g(t_1+t_2+t_3)\cong g(t_2)+\tfrac{1}{2}\xi(t_2)(t_1+t_3)^2,$$

where the root mean square fluctuation amplitude Δ is given as

$$\Delta=\left[\frac{1}{\pi}\int_0^\infty d\omega \coth(\hbar\omega/2k_BT)\tilde{\xi}_I(\omega)\right]^{1/2}=\sqrt{\xi(0)}. \tag{A2}$$

Inserting Eqs. (A1) into Eq. (11), we have

$$\Phi_1(t_3,t_2,t_1)\cong -P(0)\mu_{01}\mu_{12}\mu_{21}\mu_{10}\times\exp\{-i\bar{\omega}_{21}t_3+i\bar{\omega}_{10}t_1\}\Gamma_{\mathrm{TA}}(t_3,t_2,t_1)\times\exp\{-\tfrac{1}{2}\Delta^2t_3^2-\tfrac{1}{2}\Delta^2t_1^2+\xi(t_2)t_1t_3\},$$

$$\Phi_2(t_3,t_2,t_1)\cong -P(0)\mu_{01}\mu_{12}\mu_{21}\mu_{10}\times\exp\{-i\bar{\omega}_{21}t_3-i\bar{\omega}_{10}t_1\}\Gamma_{\mathrm{TA}}(t_3,t_2,t_1)\times\exp\{-\tfrac{1}{2}\Delta^2t_3^2-\tfrac{1}{2}\Delta^2t_1^2-\xi(t_2)t_1t_3\},$$

$$\Phi_3(t_3,t_2,t_1)\cong P(0)\mu_{01}\mu_{10}\mu_{01}\mu_{10}\times\exp\{-i\bar{\omega}_{10}t_3+i\bar{\omega}_{10}t_1\}\Gamma_{\mathrm{SE}}(t_3,t_2,t_1)\times\exp\{-\tfrac{1}{2}\Delta^2t_3^2-\tfrac{1}{2}\Delta^2t_1^2+\xi(t_2)t_1t_3\}, \tag{A3}$$

$$\Phi_4(t_3,t_2,t_1)\cong P(0)\mu_{01}\mu_{10}\mu_{01}\mu_{10}\times\exp\{-i\bar{\omega}_{10}t_3-i\bar{\omega}_{10}t_1\}\Gamma_{\mathrm{SE}}(t_3,t_2,t_1)\times\exp\{-\tfrac{1}{2}\Delta^2t_3^2-\tfrac{1}{2}\Delta^2t_1^2-\xi(t_2)t_1t_3\},$$

$$\Phi_5(t_3,t_2,t_1)\cong P(0)\mu_{01}\mu_{10}\mu_{01}\mu_{10}\times\exp\{-i\bar{\omega}_{10}t_3+i\bar{\omega}_{10}t_1\}\Gamma_{\mathrm{GB}}(t_3,t_2,t_1)\times\exp\{-\tfrac{1}{2}\Delta^2t_3^2-\tfrac{1}{2}\Delta^2t_1^2+\xi(t_2)t_1t_3\},$$

$$\Phi_6(t_3,t_2,t_1)\cong P(0)\mu_{01}\mu_{10}\mu_{01}\mu_{10}\times\exp\{-i\bar{\omega}_{10}t_3-i\bar{\omega}_{10}t_1\}\Gamma_{\mathrm{GB}}(t_3,t_2,t_1)\times\exp\{-\tfrac{1}{2}\Delta^2t_3^2-\tfrac{1}{2}\Delta^2t_1^2-\xi(t_2)t_1t_3\}.$$

Now, the population evolution period, t_2, is approximated to be the pulse delay time, i.e., $t_2\approx T$. Similar response functions were obtained by Piryatinski and Skinner recently, though they were interested in vibrational photon echo instead.[31] In order to obtain approximate 2D IR PP spectrum, the one-sided Fourier transformations in Eq. (15) are to be approximately calculated to find

$$S_{\mathrm{PP}}(\omega_{\mathrm{pr}},\omega_{\mathrm{pu}};T)\propto[\Delta^2-\xi^2(T)/\Delta^2]^{-1/2}\exp\left(-\frac{(\omega_{\mathrm{pu}}-\bar{\omega}_{10})^2}{2\Delta^2}\right)\exp\left(-\frac{[\omega_{\mathrm{pr}}-\bar{\omega}_{21}-\{\xi(T)(\omega_{\mathrm{pu}}-\bar{\omega}_{10})/\Delta^2\}]^2}{2[\Delta^2-\xi^2(T)/\Delta^2]}\right)$$
$$-[\Delta^2-\xi^2(T)/\Delta^2]^{-1/2}\exp\left(-\frac{(\omega_{\mathrm{pu}}-\bar{\omega}_{10})^2}{2\Delta^2}\right)\exp\left(-\frac{[\omega_{\mathrm{pr}}-\bar{\omega}_{10}-\{\xi(T)(\omega_{\mathrm{pu}}-\bar{\omega}_{10})/\Delta^2\}]^2}{2[\Delta^2-\xi^2(T)/\Delta^2]}\right). \tag{A4}$$

In order to obtain the above approximate expression, (i) the complementary error function (erfc) appearing after the integration over t_1 was approximated to be a unity, i.e., $\mathrm{erfc}(x)\approx 1$, (ii) the population relaxation contributions, such as $\Gamma_{\mathrm{TA}}(t_3,t_2,t_1)$, are ignored, though it is straightforward to include these terms and will cause additional frequency shifts of the maximum and minimum positions of the approximate $S_{\mathrm{PP}}(\omega_{\mathrm{pr}},\omega_{\mathrm{pu}};T)$, (iii) the pulse envelopes are assumed to be delta functions, (iv) the spectral diffusion contribution is negligibly small, and (v) the complementary error functions appear after the integration over t_3 but the real part of the complementary error function with purely imaginary argument is a unity, i.e., $\mathrm{Re}[\mathrm{erfc}(ix)]=1$ so that the final expression, Eq. (A4), for the signal does not contain any error function terms. Note that the total PP signal is nothing but a sum of two 2D Gaussian functions. The first term in Eq. (A4) is associated with the transient absorption contribution and the second with the sum of stimulated emission and ground-state bleaching contributions to the 2D PP signal. Due to the anharmonicity, i.e., $(\bar{\omega}_{10}-\bar{\omega}_{21})/2\pi c=16\ \mathrm{cm}^{-1}$, the position of the positive peak associated with the transient absorption differs from that with both the stimulated emission and ground-state bleaching. Although the approximate 2D Gaussian form of the PP spectrum is quantitatively different from the exact numerical result shown in Fig. 2, Eq. (A4) is accurate enough to prove the linear relationship between $S(T)$ and $\xi(T)$.

Let us consider $S_{\mathrm{PP}}(\omega_{\mathrm{pr}},\omega_{\mathrm{pu}};T)$ around $[\omega_{\mathrm{pu}}=(\bar{\omega}_{10}+\bar{\omega}_{21})/2$ and $\omega_{\mathrm{pu}}=\bar{\omega}_{10}]$. The root of an equation, $S_{\mathrm{PP}}(\omega_{\mathrm{pr}},\omega_{\mathrm{pu}}=\bar{\omega}_{10};T)=0$, is approximately found to be

$$\omega_{\mathrm{pr}}^{(0)}(\omega_{\mathrm{pu}}=\bar{\omega}_{10})=\frac{\bar{\omega}_{10}+\bar{\omega}_{21}}{2}. \tag{A5}$$

Now, if the pump frequency is infinitesimally shifted from $\bar{\omega}_{10}$ by δ, the new root of the equation of $S_{\mathrm{PP}}(\omega_{\mathrm{pr}},\omega_{\mathrm{pu}}=\bar{\omega}_{10}+\delta;T)=0$ is found to be

$$\omega_{\mathrm{pr}}^{(1)}(\omega_{\mathrm{pu}}=\bar{\omega}_{10}+\delta)=\frac{\bar{\omega}_{10}+\bar{\omega}_{21}}{2}+\frac{\xi(T)}{\xi(0)}\delta. \tag{A6}$$

Consequently, the inverse slope of the tangential line of the contours at $(\omega_{\mathrm{pr}}=(\bar{\omega}_{10}+\bar{\omega}_{21})/2,\omega_{\mathrm{pu}}=\bar{\omega}_{10})$ is

$$\frac{\omega_{\mathrm{pr}}^{(1)}(\omega_{\mathrm{pu}}=\bar{\omega}_{10}+\delta)-\omega_{\mathrm{pr}}^{(0)}(\omega_{\mathrm{pu}}=\bar{\omega}_{10})}{\delta}=\frac{\xi(T)}{\xi(0)}, \tag{A7}$$

so that

$$S(T)=\frac{\xi(T)}{\xi(0)}. \tag{A8}$$

Although Eq. (A8) suggests that $S(T)$ is nothing but a normalized $\xi(T)$, due to the approximations invoked in the derivation of the approximate $S_{\mathrm{PP}}(\omega_{\mathrm{pr}},\omega_{\mathrm{pu}};T)$ in Eq. (A4), Eq. (A8) should be interpreted that $S(T)$ is linearly proportional to $\xi(T)$ at best. Noting that $\xi(T)$ is real and corresponds to the correlation function of the fluctuating amide I mode frequency, one can directly obtain $\xi(T)$, which was not an experimentally measurable quantity before unless one carries out a nonlinear curve fitting of either the 2D IR photon echo or PP spectra with a simplified exponential model, by measuring the inverse slope, $S(T)$, from the experimentally measured 2D contours.

If there exists a truly static inhomogeneous contribution of which time scale is much longer than the experimentally controlled pulse delay time and its distribution is well-approximated to be a Gaussian function with the standard deviation of Δ_0, one should simply replace $\xi(T)$ with $\xi(T)+\Delta_0^2$ and Δ^2 with $\Delta^2+\Delta_0^2$ so that $S(T)=(\xi(T)+\Delta_0^2)/(\xi(0)+\Delta_0^2)$. Note that the asymptotic limit of $S(T)$ does not vanish, indicating that the 2D contours will not be vertically directed even in the limit of large T in this case of the finite static inhomogeneous limit. This is the case of Zanni *et al.*'s model[21] for $\xi(T)$ in Eq. (17) and indeed this pattern was observed in Fig. 2.

[1] A. Piryatinski, S. Tretiak, V. Chernyak, and S. Mukamel, J. Raman Spectrosc. **31**, 125 (2000).
[2] I. V. Rubtsov and R. M. Hochstrasser, J. Phys. Chem. B **106**, 9165 (2002).
[3] J. Kubelka and T. A. Keiderling, J. Am. Chem. Soc. **123**, 6142 (2001); **123**, 12048 (2001).
[4] R. Schweitzer-Stenner, Biophys. J. **83**, 523 (2002).
[5] A. M. Moran, S.-M. Park, J. Dreyer, and S. Mukamel, J. Chem. Phys. **118**, 3651 (2003).
[6] H. Torii and M. Tasumi, J. Chem. Phys. **96**, 3379 (1992).
[7] J. Torres and E. Padros, Biophys. J. **68**, 2049 (1995).
[8] J. W. Brauner, C. Dugan, and R. Mendelsohn, J. Am. Chem. Soc. **122**, 677 (2000).
[9] E. S. Manas, Z. Getahun, W. W. Wright, W. F. DeGrado, and J. M. Vanderkooi, J. Am. Chem. Soc. **122**, 9883 (2000).
[10] J. H. Werner, R. B. Dyer, R. M. Fesinmeyer, and N. H. Andersen, J. Phys. Chem. B **106**, 487 (2002).
[11] A. Xie, L. van der Meer, W. Hoff, and R. H. Austin, Phys. Rev. Lett. **84**, 5435 (2000).
[12] G. Sieler and R. Schweitzer-Stenner, J. Am. Chem. Soc. **119**, 1720 (1997).
[13] O. H. Olsen, M. R. Samuelsen, S. B. Petersen, and L. Norskov, Phys. Rev. A **39**, 3130 (1989).
[14] W. A. Herrebout, K. Clou, and H. O. Desseyn, J. Phys. Chem. A **105**, 4865 (2001).
[15] J.-H. Choi, S. Ham, and M. Cho, J. Chem. Phys. **117**, 6821 (2002); S. Cha, S. Ham, and M. Cho, *ibid.* **117**, 740 (2002); S. Ham and M. Cho, *ibid.* **118**, 6915 (2003).
[16] G. Eaton, M. C. R. Symons, and P. P. Rastogi, J. Chem. Soc., Faraday Trans. 1 **85**, 3257 (1989).
[17] P. Hamm, M. Lim, and R. M. Hochstrasser, J. Phys. Chem. B **102**, 6123 (1998).
[18] P. Hamm, M. Lim, W. F. DeGrado, and R. M. Hochstrasser, Proc. Natl. Acad. Sci. U.S.A. **96**, 2036 (1999); J. Phys. Chem. A **103**, 10049 (1999); J. Chem. Phys. **112**, 1907 (2000).
[19] C. Scheurer, A. Piryatinski, and S. Mukamel, J. Am. Chem. Soc. **123**, 3114 (2001).
[20] S. Woutersen and P. Hamm, J. Phys. Chem. B **104**, 11316 (2000); J. Chem. Phys. **115**, 7737 (2001).
[21] M. T. Zanni, M. C. Asplund, and R. M. Hochstrasser, J. Chem. Phys. **114**, 4579 (2001).
[22] M. Cho, *Advances in Multi-Photon Processes and Spectroscopy*, edited by S. H. Lin, A. A. Villaeys, and Y. Fujimura (World Scientific, Singapore, 1999), Vol. 12, p. 229.
[23] M. Cho, PhysChemCommun **5**, 40 (2002).
[24] S. Woutersen, R. Pfister, P. Hamm, Y. Mu, D. S. Kosov, and G. Stock, J. Chem. Phys. **117**, 6833 (2002).
[25] S. Woutersen, Y. Mu, G. Stock, and P. Hamm, Proc. Natl. Acad. Sci. U.S.A. **98**, 11254 (2001).
[26] S. Woutersen, Y. Mu, G. Stock, and P. Hamm, Chem. Phys. **266**, 137 (2001).
[27] K. Kwac and M. Cho, J. Chem. Phys. **119**, 2247 (2003) (companion paper).
[28] S. Ham, J.-H. Kim, H. Lee, and M. Cho, J. Chem. Phys. **118**, 3491 (2003).
[29] M. Cho, J. Chem. Phys. **115**, 4424 (2001).
[30] S. Mukamel, *Principles of Nonlinear Optical Spectroscopy* (Oxford University Press, Oxford, 1995).
[31] A. Piryatinski and J. L. Skinner, J. Phys. Chem. B **106**, 8055 (2002).
[32] M. Cho, J.-Y. Yu, T. Joo, Y. Nagasawa, S. Passino, and G. R. Fleming, J. Phys. Chem. **100**, 11944 (1996).